

## Electronic Supplementary Information

### **A Br-regulated transition metal active-sites anchoring and exposure strategy in biomass-derived carbon nanosheets for robust ORR/HER electrocatalysts at all pH values**

**Xuehui Lv,<sup>a</sup> Yanli Chen,<sup>\*a</sup> Yanling Wu,<sup>a</sup> Haoyuan Wang,<sup>a</sup> Xinlong Wang,<sup>a</sup>  
Chuangyu Wei,<sup>a</sup> Zuoxu Xiao,<sup>a</sup> Guangwu Yang<sup>a</sup> and Jianzhuang Jiang<sup>\*ab</sup>**

*a College of Science, School of Materials Science and Engineering, China University of Petroleum (East China), Qingdao, 266580, China*

*b Beijing Key Laboratory for Science and Application of Functional Molecular and Crystalline Materials, Department of Chemistry, University of Science and Technology Beijing, Beijing, 100083, China*

E-mail addresses: [yanlichen@upc.edu.cn](mailto:yanlichen@upc.edu.cn) (Y. Chen), [jianzhuang@ustb.edu.cn](mailto:jianzhuang@ustb.edu.cn) (J. Jiang).

\* Corresponding authors.

## ***1. Experimental section***

### ***1.1 Material synthesis***

#### **Preparation of 5, 10, 15, 20-tetrakis(4'-bromophenyl)porphyrin (TBrPP).<sup>1</sup>**

A solution of 4-bromobenzaldehyde (4.5 g, 25 mmol) in nitrobenzene (140 mL) and acetic acid (210 mL) was heated to 120 °C. To this solution, freshly distilled pyrrole (1.8 mL, 25 mmol) was added drop-wise. After stirring at 120 °C for 1h, the reaction mixture was cooled to room temperature. This resulting black color solution was then filtered and washed with methanol (60 mL×3). The dark violet filter cake was purified by column chromatography (silica gel, 200-300 mesh) eluting with n-hexane/dichloromethane (DCM) 2:1 follow by n-hexane/DCM 1:1 system, to give TBrPP in 21% yield. MALDI-TOF MS: calcd. for C<sub>44</sub>H<sub>26</sub>N<sub>4</sub>Br<sub>4</sub> ([M+H]<sup>+</sup>): 931; found m/z 931.5 (Fig. S1a<sup>†</sup>). <sup>1</sup>HNMR (CDCl<sub>3</sub>, 400 MHz): δ (ppm) = -2.86 (s, 2H, NH), 7.92 (d, 8H, CH<sub>Ar-phenyl</sub>), 8.06 (d, 8H, CH<sub>Ar-phenyl</sub>), 8.84 (s, 8H, CH<sub>pyrrole</sub>) (Fig. S2a<sup>†</sup>). FT-IR ν (cm<sup>-1</sup>): 3316 (NH), 3025-3065 (CH<sub>Ar</sub>), 2349 (C=N), 1217-1256 (=C-N), 1067 (C-Br), 794 (C-H<sub>pyrrole ring</sub>) (Fig. S3a<sup>†</sup>, red line). UV-vis (λ, nm, CHCl<sub>3</sub> solution): 419, 515, 549, 589 and 646.

#### **Preparation of 5,10,15,20-tetrakis(4'-bromophenyl) porphyrinato cobalt (II) (CoTBrPP).<sup>2</sup>**

150 mg TBrPP (0.16 mmol) and 940 mg of Co(OAc)<sub>2</sub>•4H<sub>2</sub>O (3.77 mmol) were placed in a 250-mL flask. After drying in vacuum for 2 h, degassed DMF (80 mL) was added under nitrogen. The reaction mixture was stirred at 150 °C overnight and cooled to room temperature. This resulting solution was then poured into water (200 mL). The

precipitate was filtered and washed by centrifugation with deionized water (60 mL×3) and MeOH (30 mL×6) until the supernatant was colorless. The residue was purified by recrystallization from chloroform and methanol twice to give CoTBrPP as a brown-red powder (125 mg, 79%). MALDI-TOF MS: calcd. for  $C_{44}H_{24}N_4Br_4Co$  ( $M^+$ ): 987; found  $m/z$  987.1 (Fig. S1b†). Compound has magnetic properties due to the introduction of metal cobalt lead to lack of distinct  $^1H$ NMR spectrogram. FT-IR  $\nu$  ( $cm^{-1}$ ): 2926-2955 ( $CH_{Ar}$ ), 2366 ( $C=N$ ), 1246 ( $=C-N$ ), 1067 ( $C-Br$ ), 1003 ( $Co-N$ ), 799 ( $C-H_{pyrrole\ ring}$ ) (Fig. S3a†, blue line). UV-*vis* ( $\lambda$ , nm,  $CHCl_3$  solution): 411 and 529.

#### **Preparation of 5, 10, 15, 20-tetraphenylporphyrin (TPP).<sup>1</sup>**

The TPP was also prepared by the same condition with TBrPP except that the benzaldehyde was used instead of 4-bromobenzaldehyde. Isolated yield: 23%. MALDI-TOF MS: calcd. for  $C_{44}H_{30}N_4$  ( $M^+$ ): 614; found  $m/z$  613.9 (Fig. S1c†).  $^1H$ NMR ( $CDCl_3$ , 400 MHz):  $\delta$  (ppm) = -2.76 (s, 2H, NH), 7.77 (d, 12H,  $CH_{Ar-phenyl}$ ), 8.22 (d, 8H,  $CH_{Ar-phenyl}$ ), 8.86 (s, 8H,  $CH_{pyrrole}$ ) (Fig. S2b†). FT-IR  $\nu$  ( $cm^{-1}$ ): 3315 (NH), 3015-3055 ( $CH_{Ar}$ ), 2352 ( $C=N$ ), 1224-1249 ( $=C-N$ ), 799 ( $C-H_{pyrrole\ ring}$ ), 725 (NH bending) (Fig. S3b†, red line). UV-*vis* ( $\lambda$ , nm,  $CHCl_3$  solution): 417, 514, 549, 589 and 646.

#### **Preparation of 5,10,15,20-tetrakis(phenyl) porphyrinato cobalt (II) (CoTPP).<sup>2</sup>**

The preparation of CoTPP is similar to CoTBrPP except that the TPP was used instead of TBrPP. Yield: 83%. MALDI-TOF MS: calcd. for  $C_{44}H_{28}N_4Co$  ( $M^+$ ): 671; found  $m/z$  670.9 (Fig. S1d†). Compound has magnetic properties due to the introduction of metal cobalt lead to lack of distinct  $^1H$ NMR spectrogram. FT-IR  $\nu$

( $\text{cm}^{-1}$ ): 3019-3058 ( $\text{CH}_{\text{Ar}}$ ), 2360 ( $\text{C}=\text{N}$ ), 1252-1297 ( $=\text{C}-\text{N}$ ), 1003 ( $\text{Co}-\text{N}$ ), 743 ( $\text{C}-\text{H}_{\text{pyrrole ring}}$ ) (Fig. S3b†, blue line). UV-*vis* ( $\lambda$ , nm,  $\text{CHCl}_3$  solution): 411 and 525.

## 1.2 Synthetic optimization

### Optimization for annealing temperature:

We should know that annealing temperature plays a significant role in the active carbon materials. In order to optimize the catalytic performance in this study, the calcination temperatures of precursor materials were changed from 700 to 800, 900 °C (The content of porphyrin precursor is fixed to the optimum content), and denoted as  $\text{CoTBrPP@bio-C-T}$  (T: 700, 800, 900). As can be seen from Fig. S5a†, the catalytic performance of carbon materials was the best one at 800 °C by measuring the linear sweep voltammetry (LSV) curves. As a result, preparation of the control sample only used a calcination treatment under 800 °C for subsequent analysis.

### Optimization for the ratio of porphyrin precursors:

The different loading dosage (mass ratio of 9:1, 5:1 and 4:1, mushroom (MR) :  $\text{CoTBrPP}$ ) of porphyrin precursor has been studied at the same pyrolysis temperature (800 °C) for the purpose of preparing the final catalysts, and denoted as  $\text{CoTBrPP@bio-C-P}$  (P: 9, 5 and 4). From the Fig. S5b†, the performance presents first increase and later decrease trend with increased in loading dosage. It was also found that when the mass ratio of MR:  $\text{CoTBrPP}$  is 5:1, the carbon materials obtained exhibited the optimal catalytic performance. Consequently, we chose this proportion as the final loading to prepare the controlled samples and for subsequent analysis.

### ***1.3 Characterization***

X-ray diffraction (XRD) analysis was performed on a Rigaku Ultima IV X-ray diffractometer using a Cu K $\alpha$  source (40 kV, 40 mA). The morphology and structure of the materials were measured by field-emission scanning electron microscope (SEM, Quant 250FEG) equipped with an energy-dispersive X-ray (EDX) detector and high-resolution transmission electron microscope (HRTEM, JEM-2100F) at 200 kV. Fourier transform infrared (FT-IR) spectroscopy measurement was recorded at room temperature on the Bruker Tensor II spectrometer with 2 cm<sup>-1</sup> resolution in the form of KBr pellet. Ultraviolet-visible spectroscopy (UV-*vis*) was operated on a Hitachi U-3900 spectrophotometer. High-resolution MALDI-TOF mass spectrum was recorded on a Bruker BIFLEX III ultra-high resolution Fourier transform ion cyclotron resonance (FT-ICR) mass spectrometer with alpha-cyano-4-hydroxycinnamic acid as matrix. <sup>1</sup>H NMR spectra were taken on the Bruker DPX 400 spectrometer (400 MHz) in CDCl<sub>3</sub>. Thermogravimetric (TG) analysis of porphyrin precursors were studied on a simultaneous DSC-TGA SDT 650 analyzer under N<sub>2</sub> flowing with a 5 °C min<sup>-1</sup> heating rate. X-ray photoelectron spectroscopy (XPS) analysis was carried out using an Axis Ultra instrument from Kratos with monochromatic Al K $\alpha$  radiation. Raman spectroscopy of the samples was measured with a laser Raman microscope system (Nanophoton RAMANtouch) excited with 532 nm. N<sub>2</sub> adsorption-desorption isotherms were analyzed through a Micromeritics ASAP 2060 analyzer at 77 K and the specific surface area of the materials were calculated based on the Brunauer-

Emmett-Teller (BET) method, the total pore volume were estimated from single point adsorption at a relative pressure  $P/P_0$  of 0.995 and the pore size distributions were calculated by means of Barrett-Joyner-Halenda (BJH) method. The contact angle analysis was carried out using an OCAH200 optical contact angle measuring instrument (Dataphysics, Germany) at ambient temperature. The ball-milling treatment was carried out in a XQM-2 planetary ball mill from Changsha Tencan technology Co., Ltd. Both the grinding jar and ball are made of alumina.

#### ***1.4 Electrochemical measurements***

The rotary disk electrode (RDE, Pine Research Instrumentation, Inc.) with a Pine Modulated Speed Rotator (Pine Research Instrumentation, Inc.) measurements described in this study was used to measure cyclic voltammetry (CV) and LSV. The electrocatalytic activity of CoTBrPP@bio-C and CoTPP@bio-C for oxygen reduction was studied in an oxygen saturated condition using a rotating ring-disk electrode (RRDE, Pine Research Instrumentation, Inc.) at a rotation speed of 1600 rpm. All the electrochemical measurements were measured by the aid of a CHI 760E electrochemical analyzer in a three-electrode electrochemical cell at room temperature (*ca.* 25°C). The glassy carbon rotating disk (GC, 5.0 mm in diameter) modified with various electrocatalysts and silver/silver chloride (Ag/AgCl, in saturated 3M KCl solution) were used as the working and reference electrodes, respectively. For ORR, platinum foil and graphite rod served as the auxiliary electrode in alkaline medium and acid medium. For HER, graphite rod was used as the auxiliary electrode. All

potentials of the working electrode were converted *versus* reversible hydrogen electrode (RHE) using the following equation:

$$E_{(\text{RHE})} = E_{\text{Ag}/\text{AgCl}} + 0.0592 \text{ pH} + E_{\text{Ag}/\text{AgCl}}^{\ominus}$$

where  $E_{\text{Ag}/\text{AgCl}}^{\ominus}$  is 0.1989 V.

In a typical procedure, the GC electrode in both cases was prepared by mixing 5.0 mg of as-prepared samples in 0.8 mL of an isopropyl alcohol solution containing 40  $\mu\text{L}$  of a 5 wt% Nafion solution and then ultrasonicated for 30 min to form a homogeneous slurry. Then 10  $\mu\text{L}$  of ink was pipetted onto a polished GC electrode surface and dried naturally to form a homogeneous membrane. The general loading of the electrocatalysts on the working electrode is 0.30 mg  $\text{cm}^{-2}$ . For comparison, 5.0 mg of commercial available Pt/C (20 wt%) was also dispersed on the GC electrode in the same way.

Before the ORR activity measurements, the electrolyte solution was degassed with high purity oxygen or nitrogen at least 30 min. All CV curves were conducted at a scan rate of 50  $\text{mV s}^{-1}$  and LSV curves were measured with 5  $\text{mV s}^{-1}$  in 0.1 M KOH, 0.5 M  $\text{H}_2\text{SO}_4$  and PBS (pH = 7.3). The diffusion-limited current density ( $J_L$ ) was recorded at 0.2 V vs. RHE. The effective active surface areas (ECSA) of the electrocatalysts were collected by measuring the CV curves at different scan rates (40-140  $\text{mV s}^{-1}$ ) in order to estimate the degree of exposed electrochemically active sites on the working electrode. The stability of the active materials was conducted in  $\text{O}_2$ -saturated 0.1 M KOH solution at 1600 rpm *via* i-t (current *versus* time) curve. Accelerated durability tests were conducted by cycling the catalyst with the potentials

range from 0.6 V to 1.1 V at a scan rate of 50 mV s<sup>-1</sup> under O<sub>2</sub>-saturated 0.1 M KOH and 0.5 M H<sub>2</sub>SO<sub>4</sub> electrolyte. Electrochemical impedance spectra (EIS) measurements have been studied under an open-circuit potential (OCP) over a frequency range of 0.1-10<sup>5</sup> Hz and amplitude applied voltage of 5 mV. Methanol tolerance tests were carried out by chronoamperometry measurements in the case of injecting the 3.0 M methanol into the electrolyte.

LSV for HER were performed with a scan rate of 5 mV s<sup>-1</sup> in N<sub>2</sub>-saturated 1.0 M KOH, 0.5 M H<sub>2</sub>SO<sub>4</sub> and PBS (pH = 7.3) solution at a rotating rate of 0 rpm under the room temperature. All data are presented with *iR* compensation.

### ***1.5 Assembly of typical Zn-air batteries***

Zinc-air battery tests: All Zn-air batteries were evaluated under ambient conditions. This device was fabricated using the CoTBrPP@bio-C catalyst dispersed on the carbon paper as the air cathode, a polished Zn foil as the anode and 6 M KOH solution as electrolyte respectively. For comparison purposes, CoTPP@bio-C and commercial Pt/C were also tested as the air cathode under the same test conditions. The polarization curves were recorded by linear sweep voltammetry (5 mV s<sup>-1</sup>) on a CHI 760E electrochemical platform. The cathode was prepared by loading CoTBrPP@bio-C, CoTPP@bio-C and Pt/C catalysts on the carbon paper (catalyst loading amount of 1.0 mg cm<sup>-2</sup>).

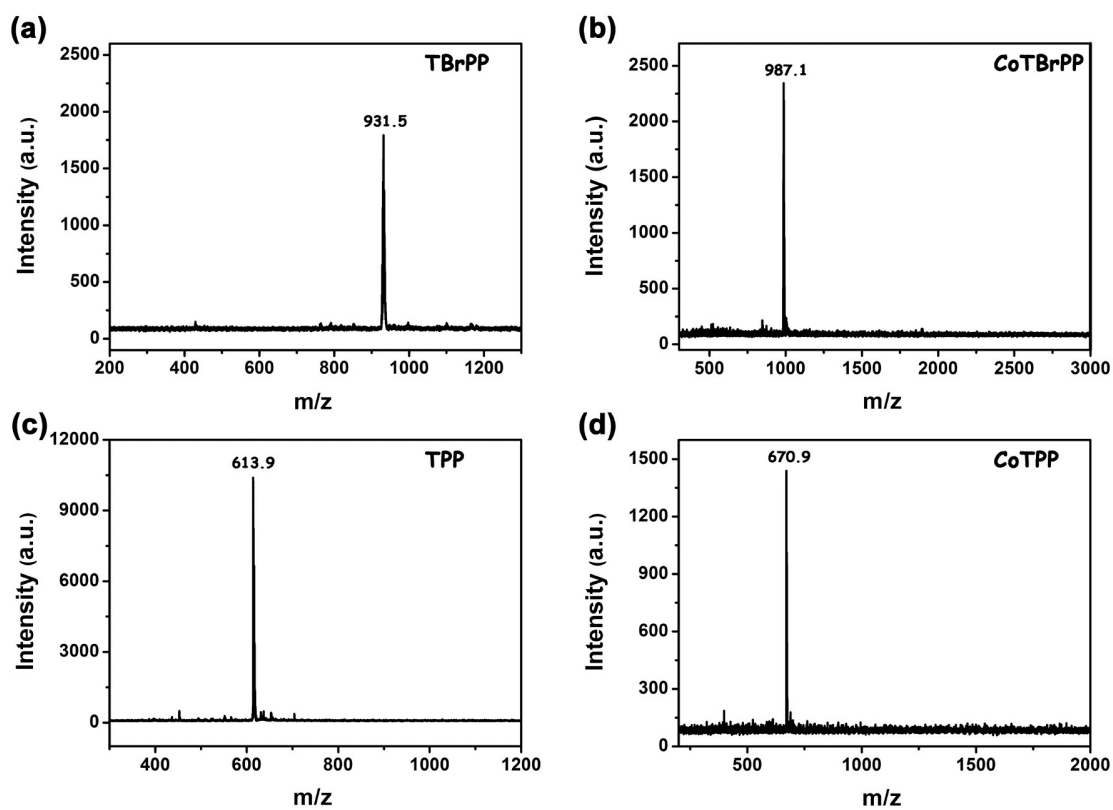


Fig. S1. MALDI-TOF mass spectra for a) TBrPP, b) CoTBrPP, c) TPP and d) CoTPP.

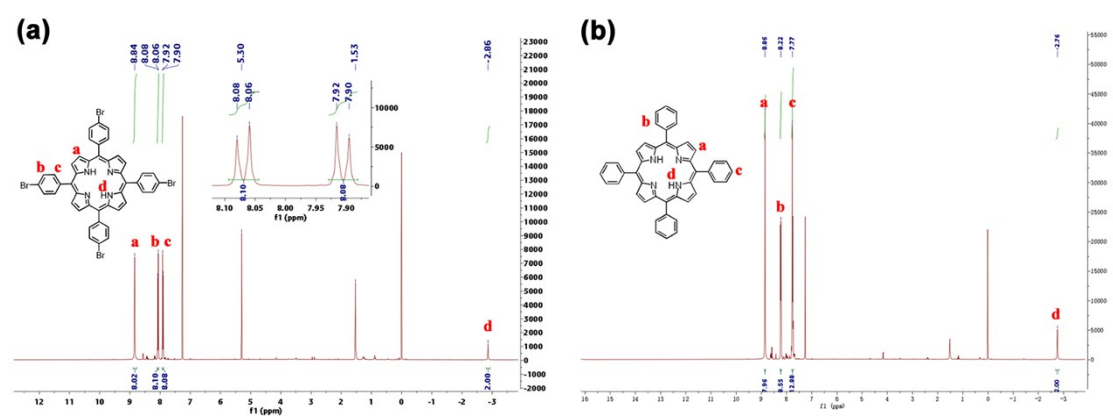
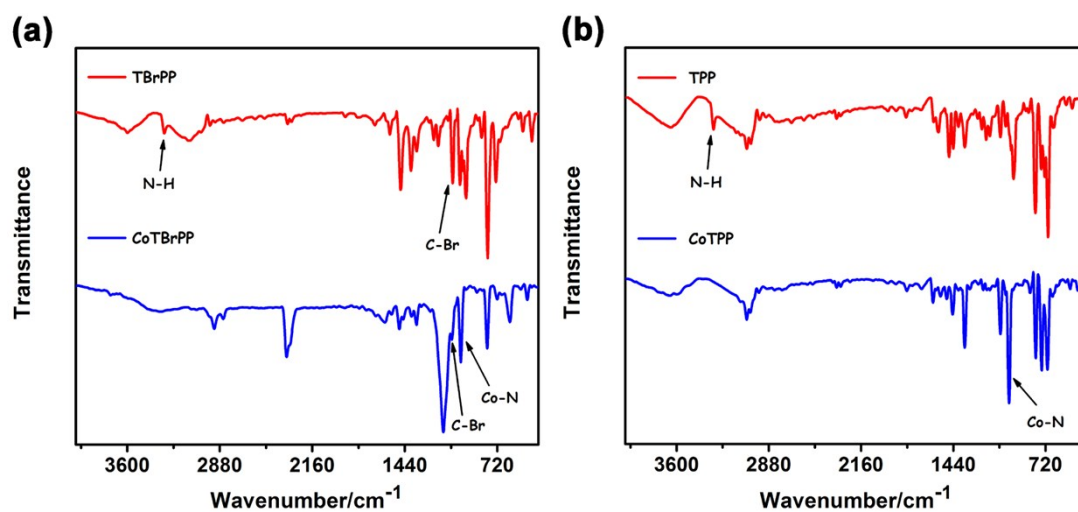
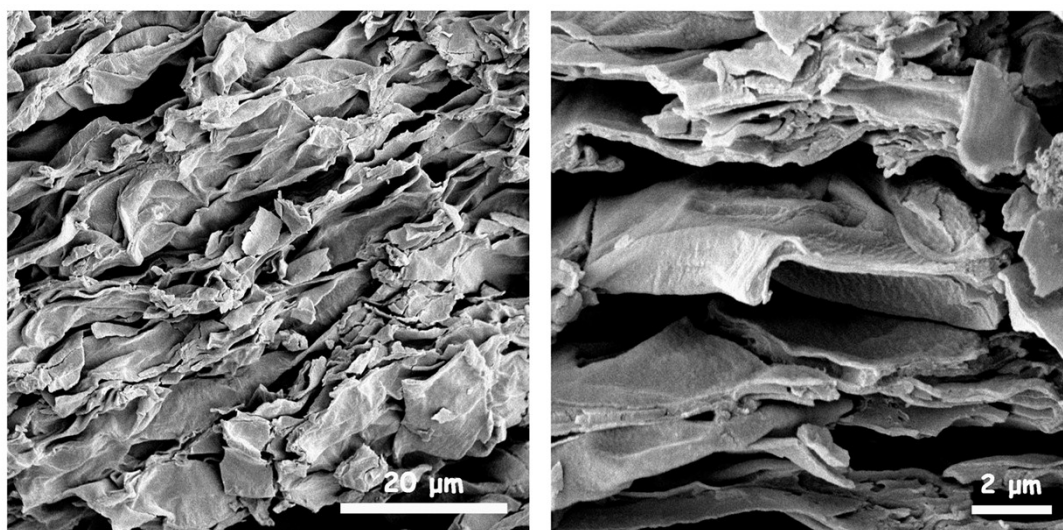


Fig. S2. <sup>1</sup>H NMR spectra for a) TBrPP and b) TPP.



**Fig. S3.** FTIR spectra for a) TBrPP and CoTBrPP, b) TPP and CoTPP.



**Fig. S4.** SEM images of the MR powder.

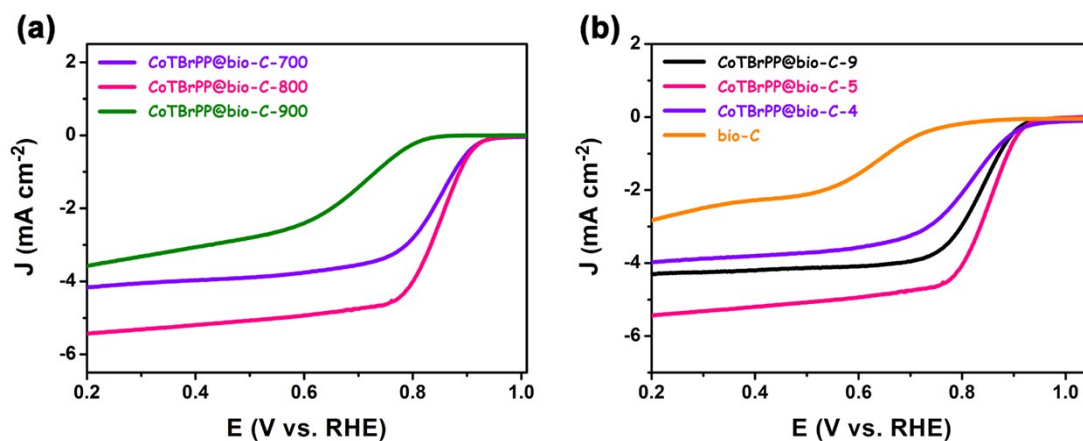


**Fig. S5.** LSV curves at 1600 rpm of the a) CoTBrPP@bio-C under different annealing temperatures, b) CoTBrPP@bio-C prepared by varies content of porphyrin precursor in O<sub>2</sub>-saturated 0.1 M KOH electrolyte with a sweep rate of 5 mV s<sup>-1</sup>, respectively.

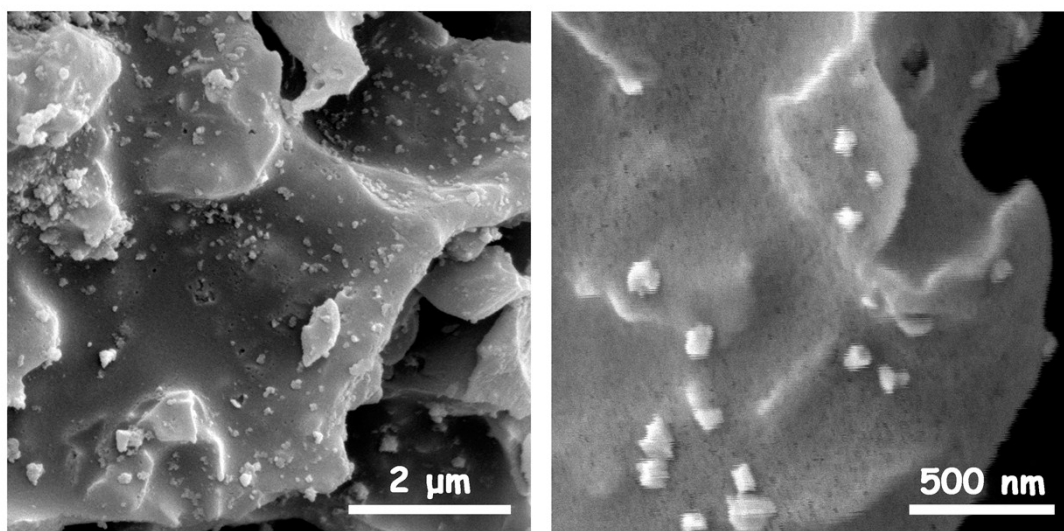


**Fig. S6.** SEM images of the CoTPP@bio-C.

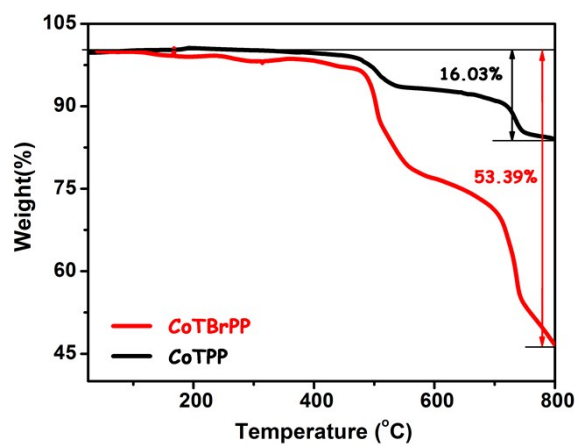


**Fig. S7.** Thermogravimetric (TG) curves for CoTBrPP (red line) and CoTPP (black line).

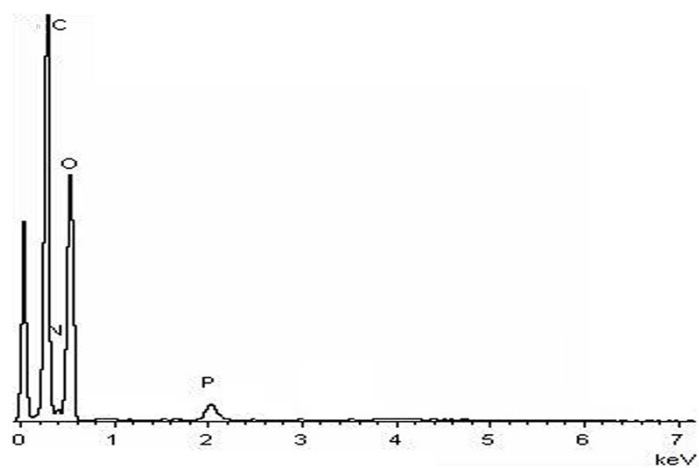


**Fig. S8.** The EDX spectrum of pure MR powder.

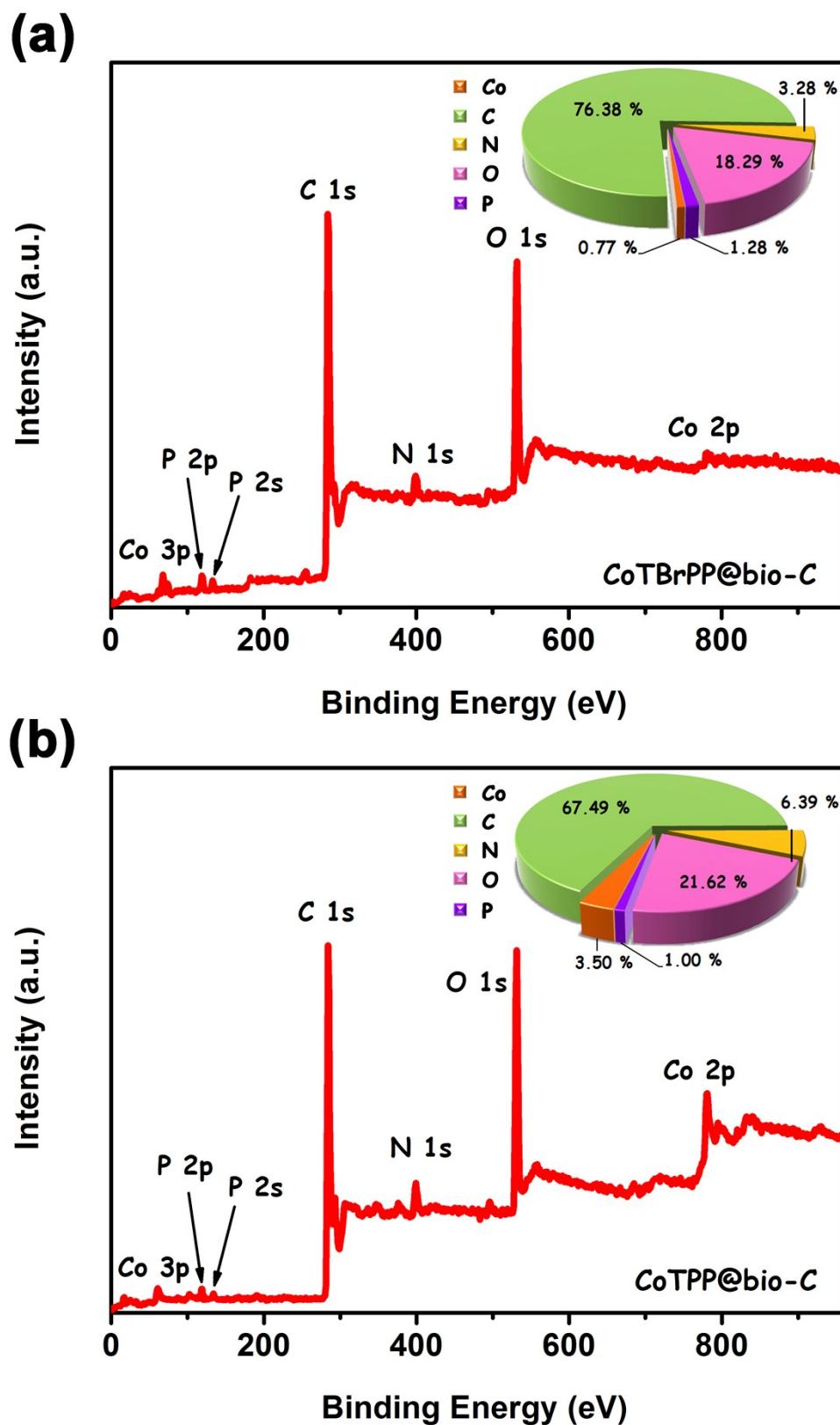


**Fig. S9.** XPS survey spectra of the a) CoTBrPP@bio-C and b) CoTPP@bio-C. Inset: the percentage of surface elements determined by XPS.

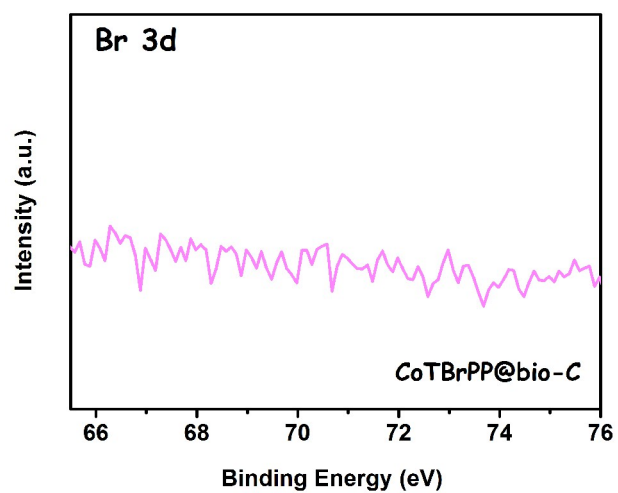


**Fig. S10.** High-resolution Br 3d XPS spectra of the CoTBrPP@bio-C.

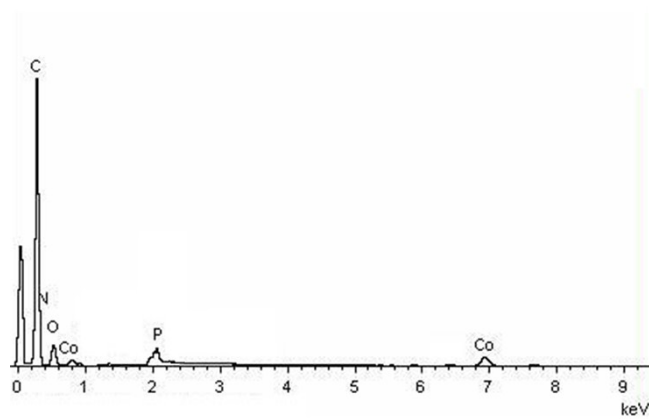


**Fig. S11.** The EDX spectrum of CoTBrPP@bio-C.

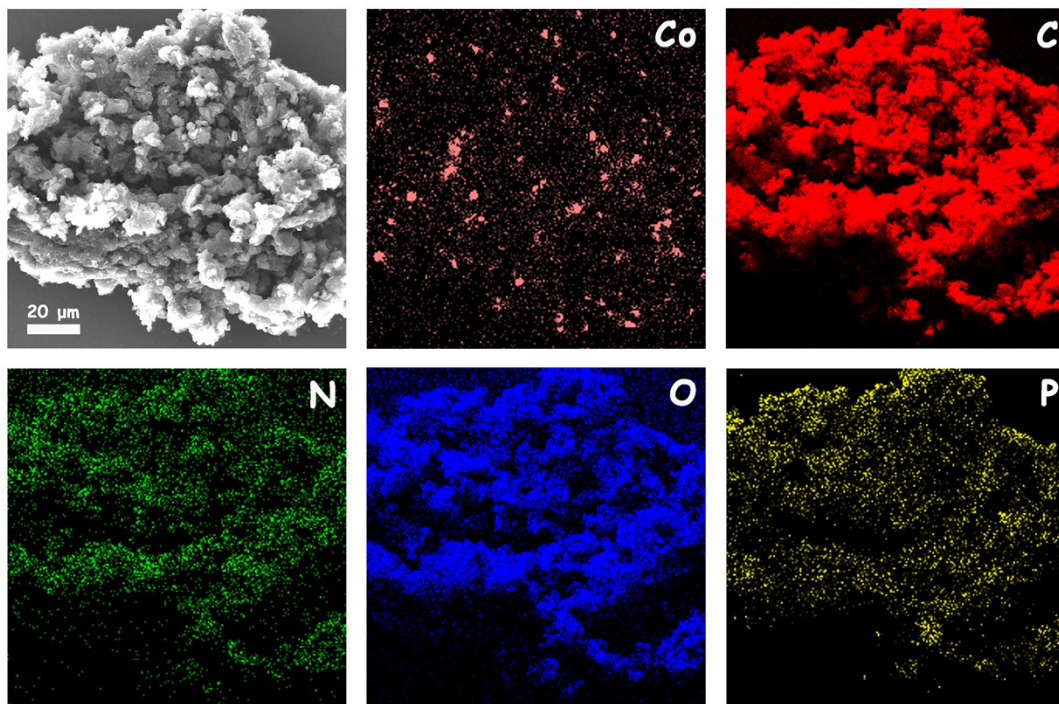


**Fig. S12.** SEM image and corresponding elemental mapping diagrams of CoTBrPP@bio-C.

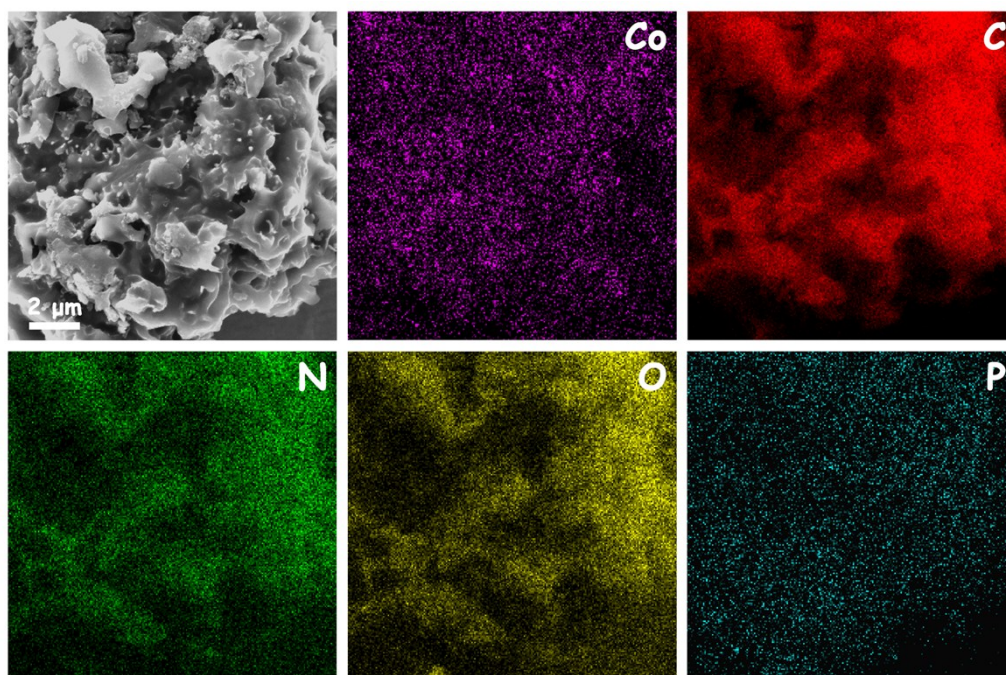


**Fig. S13.** SEM image and corresponding elemental mapping diagrams of CoTPP@bio-C.

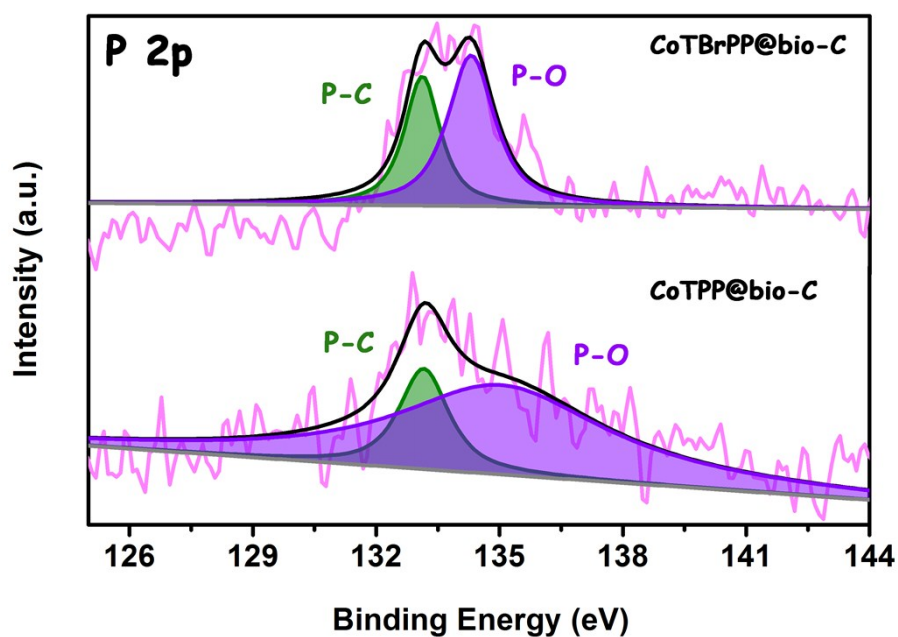


**Fig. S14.** High-resolution XPS spectra P 2p of the CoTBrPP@bio-C and CoTPP@bio-C.

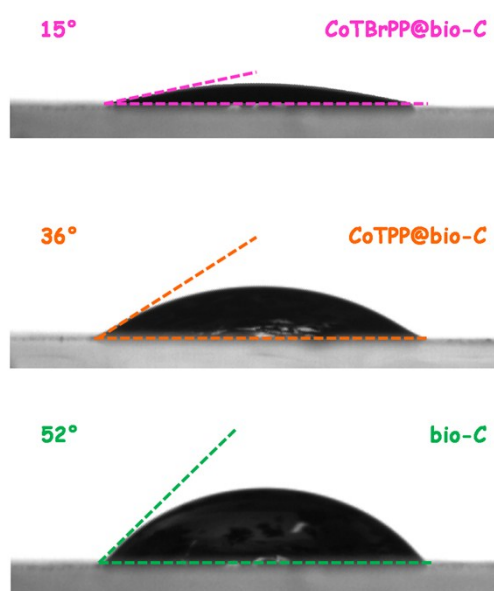


**Fig. S15.** Contact angle of CoTBrPP@bio-C, CoTPP@bio-C and bio-C.

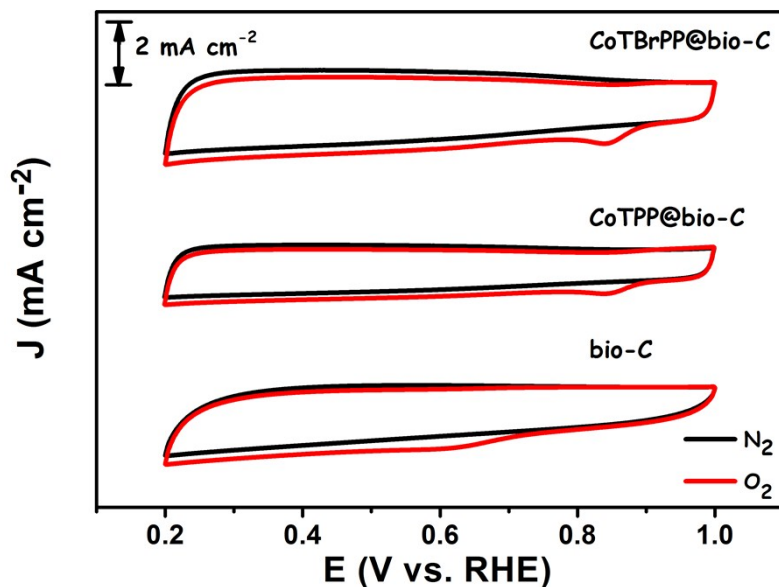


**Fig. S16.** CV curves of the CoTBrPP@bio-C, CoTPP@bio-C and bio-C in O<sub>2</sub>-saturated (red line) and N<sub>2</sub>-saturated (black lines) 0.1 M KOH at 50 mV s<sup>-1</sup>, respectively.

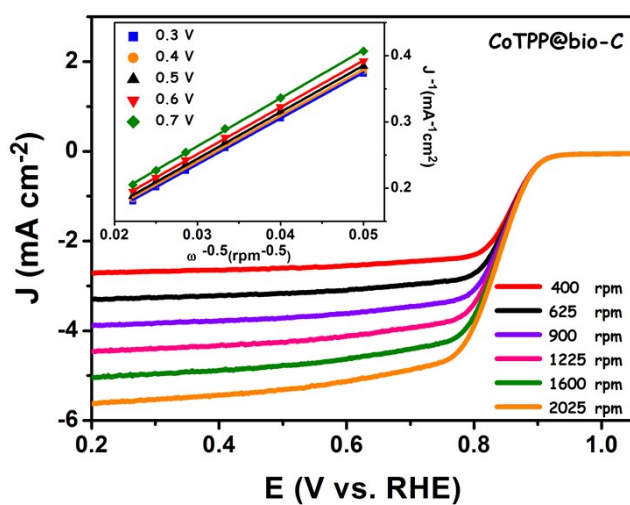


**Fig. S17.** LSV curves of the CoTPP@bio-C at various rotating speeds in 0.1 M KOH.

Inset: K-L plots of the CoTPP@bio-C at various potentials.

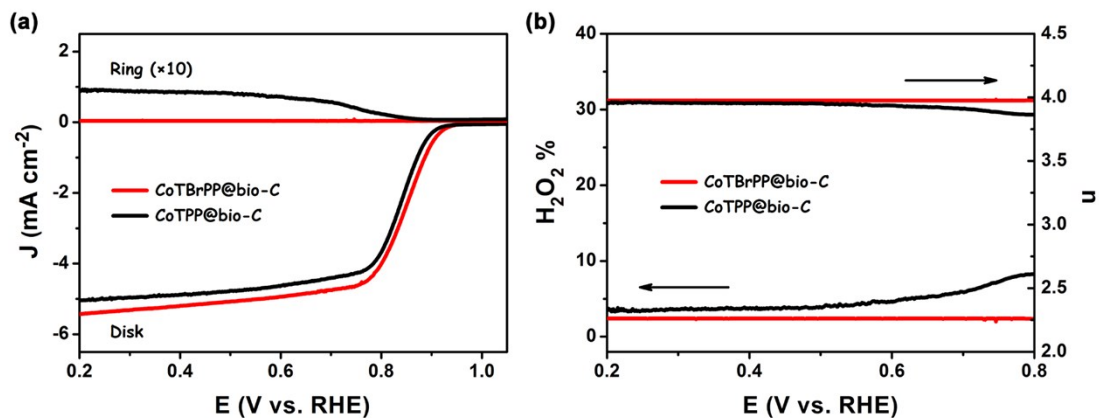


**Fig. S18.** a) RRDE voltammograms and b)  $\text{H}_2\text{O}_2$  yield ( $\text{H}_2\text{O}_2$  %) as well as the calculated electron transfer number ( $n$ ) of  $\text{CoTBrPP@bio-C}$  and  $\text{CoTPP@bio-C}$ .

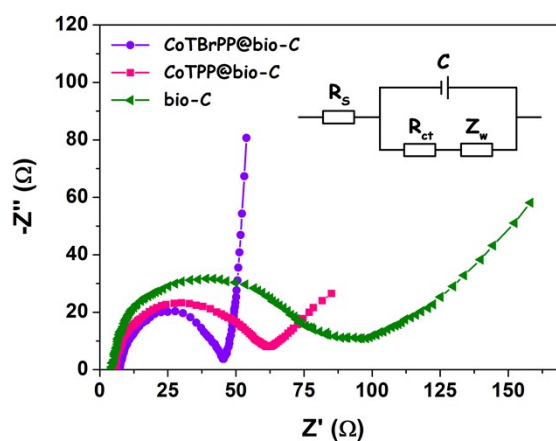


**Fig. S19.** Nyquist plots of  $\text{CoTBrPP@bio-C}$ ,  $\text{CoTPP@bio-C}$ , and  $\text{bio-C}$  catalysts-modified electrodes in 0.1 M KOH solution (Inset: corresponding equivalent circuit).

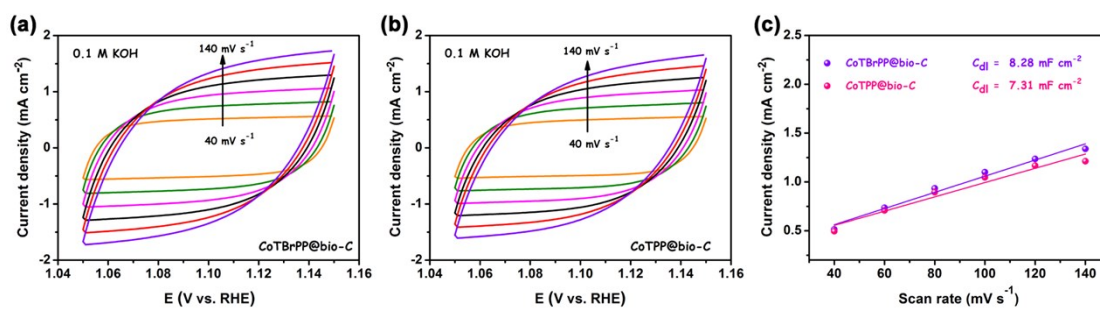


**Fig. S20.** Cyclic voltammograms (CV) at various scan rates of a) CoTBrPP@bio-C and b) CoTPP@bio-C in 0.1 M KOH solution. c) The electrochemical double-layer capacitance ( $C_{dl}$ ) of CoTBrPP@bio-C and CoTPP@bio-C in 0.1 M KOH electrolyte.

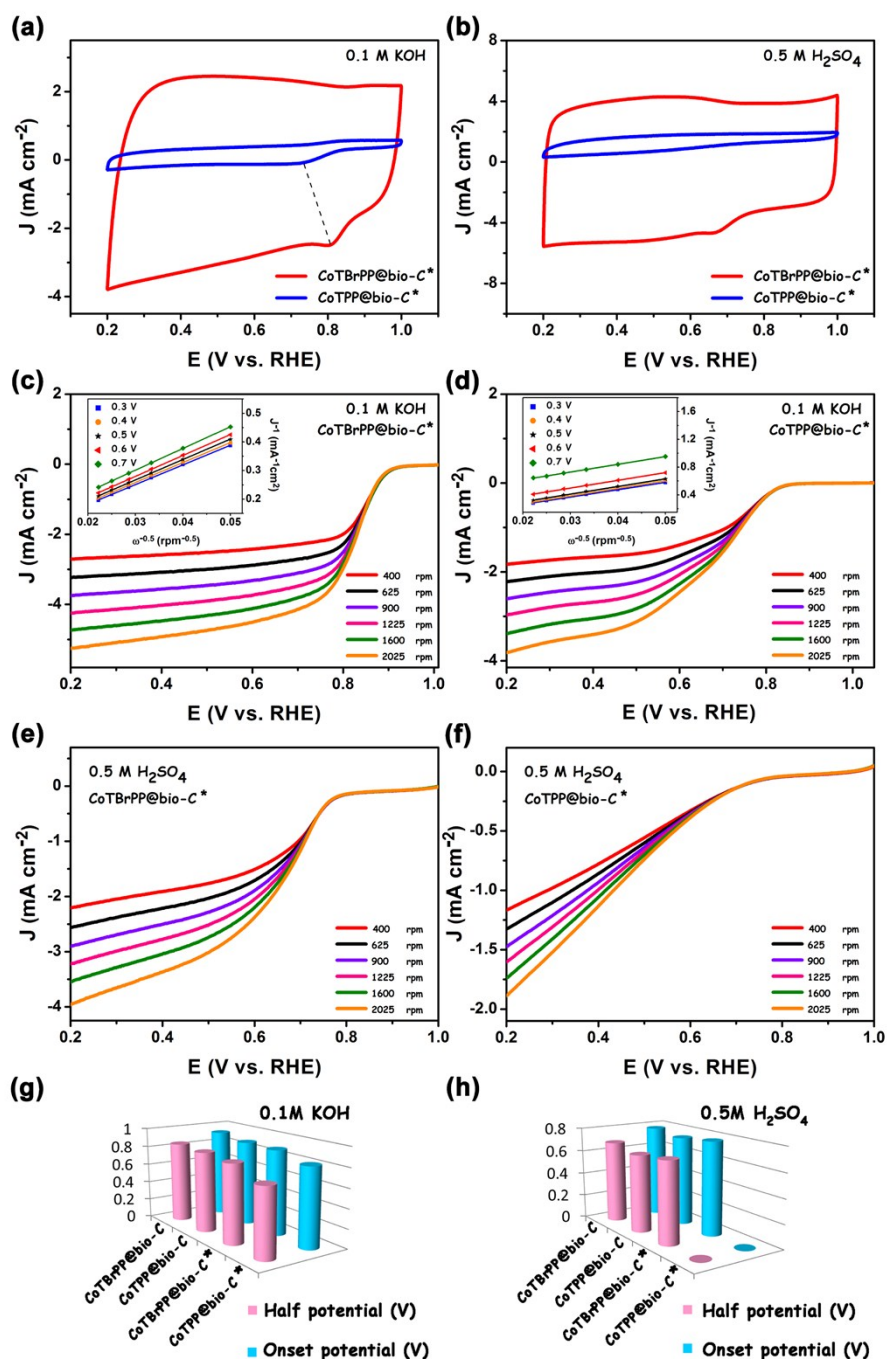


**Fig. S21.** CV curves of the CoTBrPP@bio-C\* and CoTPP@bio-C\* in O<sub>2</sub>-saturated a) 0.1 M KOH and b) 0.5 M H<sub>2</sub>SO<sub>4</sub>. LSV curves of CoTBrPP@bio-C\* and CoTPP@bio-C\* at various rotating speeds in c), d) 0.1 M KOH and e), f) 0.5 M H<sub>2</sub>SO<sub>4</sub>. Inset c) and d): the K-L plots. Comparison of activities (onset potential and ESI-19

half potential) for CoTBrPP@bio-C and various comparative catalysts in g) 0.1 M KOH and h) 0.5 M H<sub>2</sub>SO<sub>4</sub> electrolyte, respectively, (“\*” stands for the corresponding samples after acid etching).

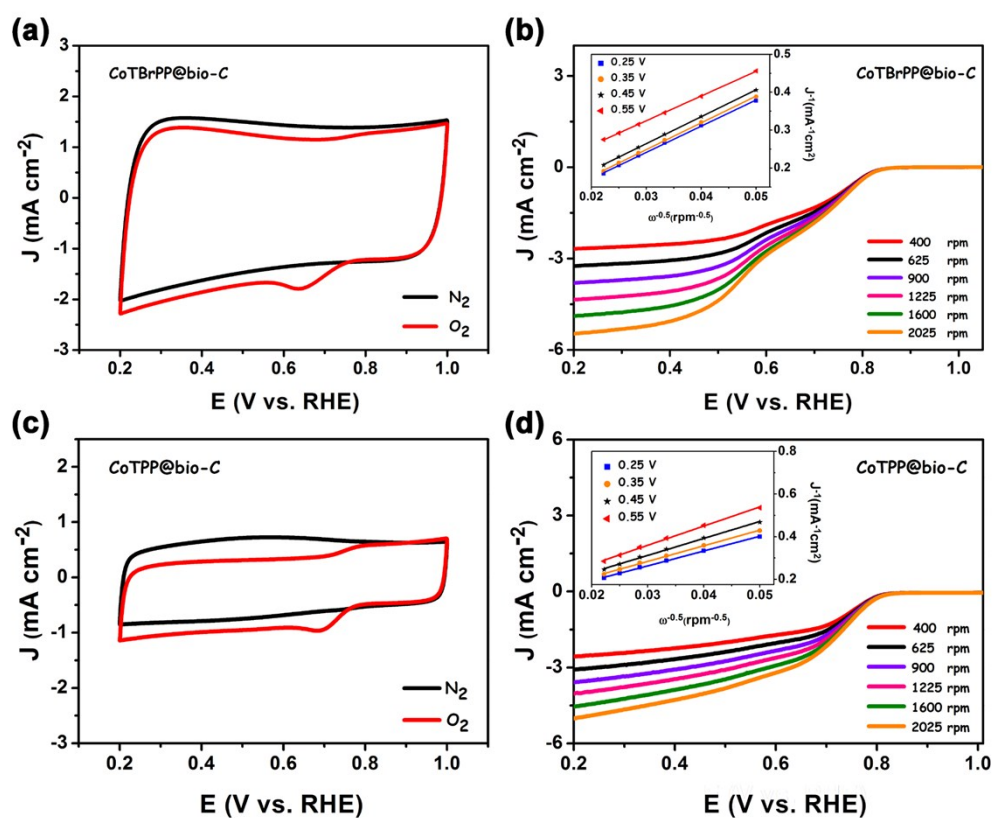


**Fig. S22.** CV curves of the a) CoTBrPP@bio-C and c) CoTPP@bio-C in  $O_2$ -saturated (red lines) and  $N_2$ -saturated (black lines) neutral PBS phosphate buffer solution (pH = 7.3) at  $50 \text{ mV s}^{-1}$ , respectively. LSV curves of the b) CoTBrPP@bio-C and d) CoTPP@bio-C at various rotating speeds in PBS.

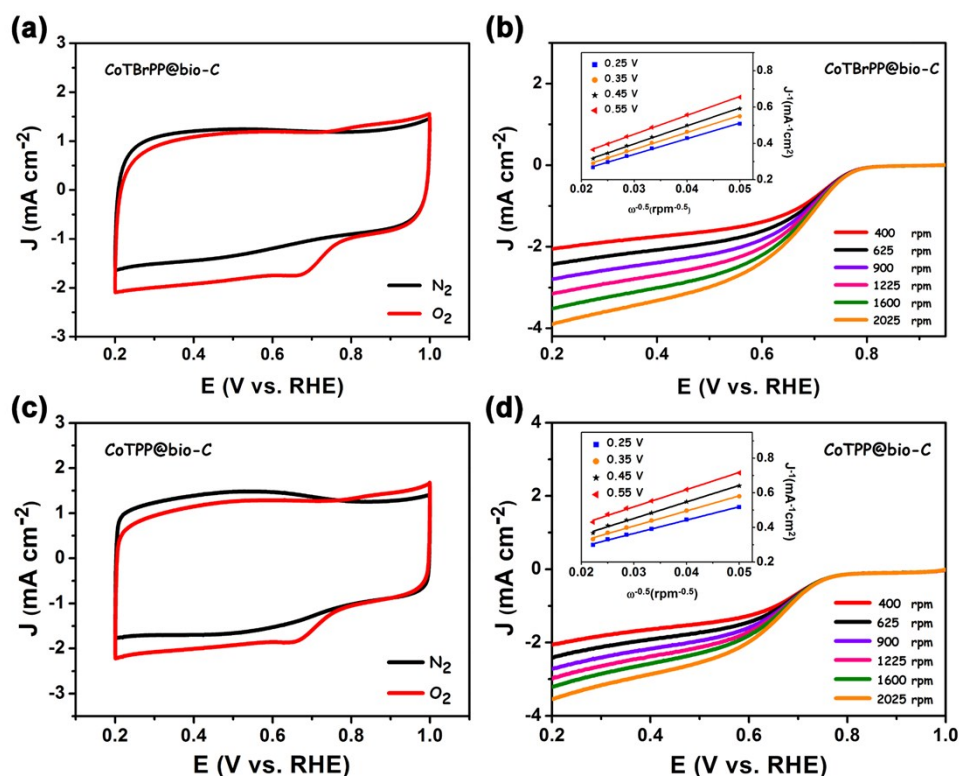


**Fig. S23.** CV curves of the a) CoTBrPP@bio-C and c) CoTPP@bio-C in O<sub>2</sub>-saturated (red lines) and N<sub>2</sub>-saturated (black lines) 0.5 M H<sub>2</sub>SO<sub>4</sub> at 50 mV s<sup>-1</sup>, respectively. LSV curves of the b) CoTBrPP@bio-C and d) CoTPP@bio-C at various rotating speeds in 0.5 M H<sub>2</sub>SO<sub>4</sub>.

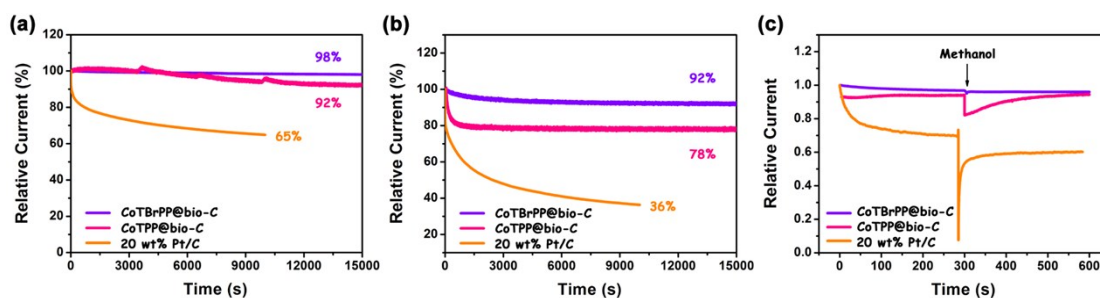


**Fig. S24.** Amperometric i-t curves of CoTBrPP@bio-C, CoTPP@bio-C and 20 wt% Pt/C in a) 0.1 M KOH electrolyte and b) 0.5 M H<sub>2</sub>SO<sub>4</sub> electrolyte. c) Chronoamperometric responses of CoTBrPP@bio-C, CoTPP@bio-C and 20 wt% Pt/C upon the addition of 3 M methanol into O<sub>2</sub>-saturated 0.1 M KOH.

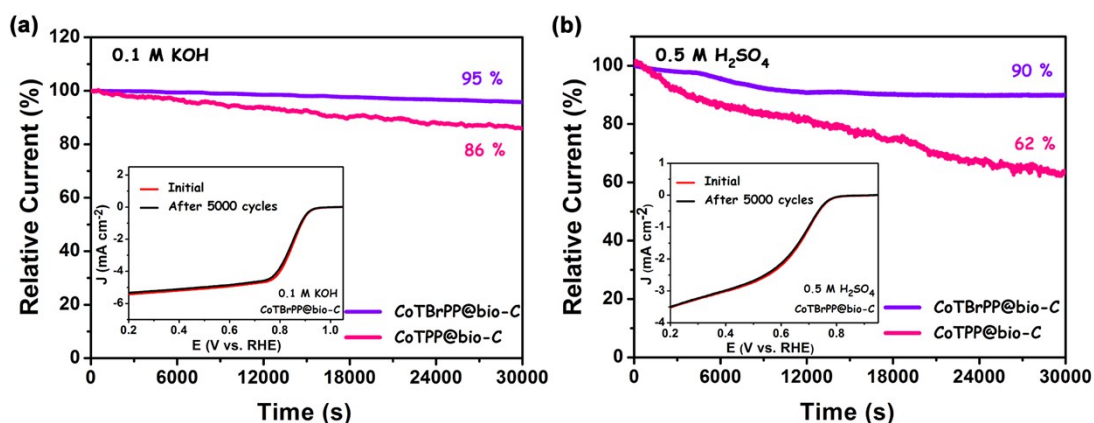


**Fig. S25.** Amperometric i-t curves of CoTBrPP@bio-C and CoTPP@bio-C in a) 0.1 M KOH electrolyte and b) 0.5 M H<sub>2</sub>SO<sub>4</sub> electrolyte over 30000 s. Inset: ORR LSV curves recorded for CoTBrPP@bio-C before and after 5000 cycles.

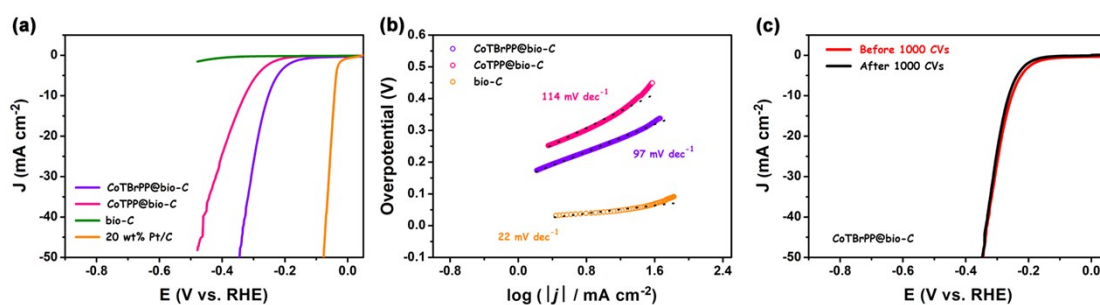


**Fig. S26.** a) LSV curves of CoTBrPP@bio-C, the comparative catalysts, and 20 wt% Pt/C in 0.5 M H<sub>2</sub>SO<sub>4</sub> (5 mV s<sup>-1</sup>). b) Tafel plots of CoTBrPP@bio-C, CoTPP@bio-C and 20 wt% Pt/C derived from the LSV data. c) Polarization curves of CoTBrPP@bio-C before and after 1000 CV cycles in 0.5 M H<sub>2</sub>SO<sub>4</sub>.

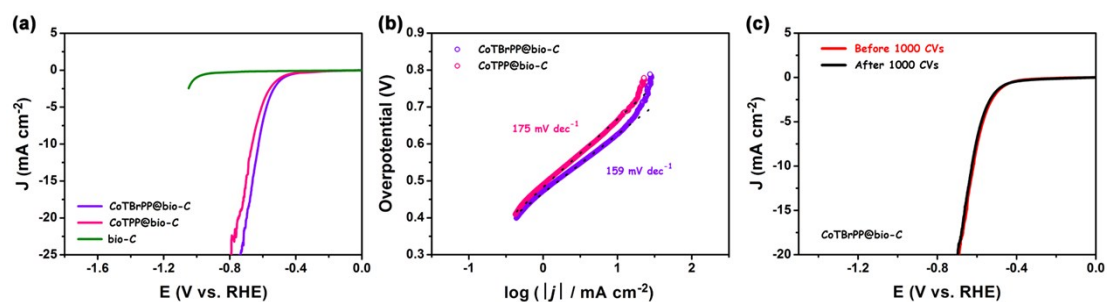


**Fig. S27.** a) LSV curves of CoTBrPP@bio-C and the comparative catalysts in neutral PBS phosphate buffer solution ( $\text{pH} = 7.3$ ) ( $5 \text{ mV s}^{-1}$ ). b) Tafel plots of CoTBrPP@bio-C and CoTPP@bio-C derived from the LSV data. c) Polarization curves of CoTBrPP@bio-C before and after 1000 CV cycles in PBS.

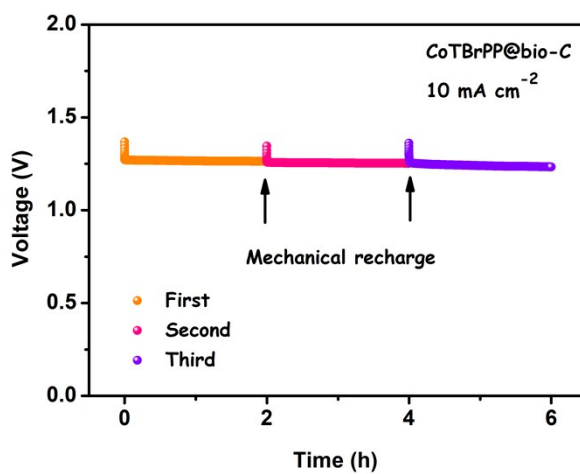


**Fig. S28.** Long-time discharge curve of the battery with a CoTBrPP@bio-C electrode at a current rate of  $10 \text{ mA cm}^{-2}$ . The arrow indicates the point where the zinc and electrolyte were replaced.

**Table S1.** The specific surface area (SSA) of BET, average pore diameter and pore volume of bio-C, CoTPP@bio-C and CoTBrPP@bio-C, respectively.

Sample	SSA of BET (m <sup>2</sup> /g)	Average pore diameter (nm)	Pore volume (cm <sup>3</sup> /g)
bio-C	1.4	13.6	0.003
CoTPP@bio-C	98.1	4.10	0.077
CoTBrPP@bio-C	604.0	4.75	0.442

**Table S2.** The ORR performance of CoTBrPP@bio-C, CoTPP@bio-C and corresponding sample obtained after acid pickling in different electrolyte, respectively.

<b>Sample</b>	<b>Onset potential (V)</b>	<b>Half wave potential (V)</b>	<b>Current density (mA cm<sup>-2</sup>)</b>	<b>Electrolyte</b>
CoTBrPP@bio-C	0.93	0.85	5.43	0.1 M KOH
CoTPP@bio-C	0.89	0.84	5.04	0.1 M KOH
CoTBrPP@bio-C	0.78	0.69	3.50	0.5 M H <sub>2</sub> SO <sub>4</sub>
CoTPP@bio-C	0.75	0.65	3.21	0.5 M H <sub>2</sub> SO <sub>4</sub>
CoTBrPP@bio-C	0.83	0.65	5.08	PBS
CoTPP@bio-C	0.81	0.69	4.55	PBS
CoTBrPP@bio-C*	0.89	0.82	4.75	0.1 M KOH
CoTPP@bio-C*	0.82	0.71	3.39	0.1 M KOH
CoTBrPP@bio-C*	0.78	0.68	3.57	0.5 M H <sub>2</sub> SO <sub>4</sub>
CoTPP@bio-C*	N	N	N	0.5 M H <sub>2</sub> SO <sub>4</sub>

Note on table:

- (\*) The corresponding sample obtained after acid pickling.
- (N) No electrocatalytic activity.

**Table S3.** Comparison of the ORR performance for CoTBrPP@bio-C and other TMN/TMC-based catalysts at 1600 rpm in 0.1 M KOH.

<b>Catalysts</b>	<b>Loading mass (mg cm<sup>-2</sup>)</b>	<b>Onset potential (V)</b>	<b>Half-wave potential (V)</b>	<b>Current density (mA cm<sup>-2</sup>)</b>	<b>References</b>
CoTBrPP@bio-C	0.30	0.93	0.85	5.43	This work
CoTPP@bio-C	0.30	0.89	0.84	5.04	This work
Co <sub>4</sub> N@NC-m	1.00	0.98	0.87	NA	3
Fe-N/TiC	0.35	0.83	0.70	4.7	4
N-CDs@WN	0.49	0.95	0.78	4.66	5
TiN HSs-325	NA	0.85	NA	4.50	6
Fe <sub>3</sub> N@N-C	0.26	0.995	0.849	NA	7
Ni <sub>3</sub> FeN@Co <sub>3</sub> N-CNF	0.40	0.93	0.81	NA	8
NiO/CoN PINWs	0.20	0.89	0.68	NA	9
Mo <sub>2</sub> C-C-5	0.40	0.832	0.713	5.52 (at 0.165 V)	10

Note on table:

(NA) not attained.

**Table S4.** The Comparison of HER performance of CoTBrPP@bio-C and CoTPP@bio-C in different electrolyte, respectively.

<b>Catalysts</b>	<b>Electrolyte</b>	<b>Onset potential (V)</b>	<b>Overpotential (<math>\eta_{j=10\text{ mA cm}^{-2}}</math>, V)</b>	<b>Tafel slope (mV dec<sup>-1</sup>)</b>
CoTBrPP@bio-C	1 M KOH	0.14	0.22	80
CoTPP@bio-C	1 M KOH	0.20	0.30	109
CoTBrPP@bio-C	0.5 M H <sub>2</sub> SO <sub>4</sub>	0.15	0.25	97
CoTPP@bio-C	0.5 M H <sub>2</sub> SO <sub>4</sub>	0.22	0.33	114
CoTBrPP@bio-C	PBS	0.47	0.63	159
CoTPP@bio-C	PBS	0.49	0.66	175

**Table S5.** Comparison of the HER performance for CoTBrPP@bio-C and other TMN/TMC-based or Co-based catalysts in 1 M KOH.

<b>Catalysts</b>	<b>Loading mass</b>	<b>Overpotential</b>	<b>Tafel slope</b>	<b>References</b>
	<b>(mg cm<sup>-2</sup>)</b>	<b>(<math>\eta_{j=10\text{ mA cm}^{-2}}</math>, V)</b>	<b>(mV dec<sup>-1</sup>)</b>	
CoTBrPP@bio-C	0.30	0.22	80	This work
CoTPP@bio-C	0.30	0.30	109	This work
TiO <sub>2</sub> C@CN <sub>x,950</sub>	0.283	0.495	133	11
Co@N-CNTF-2	0.28	0.260	NA	12
1% Co-N-GDY	0.40	0.271	132	13
Co-NC	0.40	0.242	96	14
Al-Fe <sub>2</sub> N/Fe <sub>3</sub> N	NA	0.299	66	15
CoN-300/CC	NA	0.236	117.3	16
Co/CoP-5	0.22	0.253	73.8	17
Ni <sub>3</sub> FeN-NPs	0.20	0.238	46	18
CoNS-C	0.30	0.251	91	19
CoNC/GD	0.286	0.284	115	20

Note on table: (NA) not attained.

**Table S6.** A comparison of the performance of primary Zn-air batteries with various electrocatalysts.

<b>Catalyst</b>	<b>Loading</b>	<b>Peak power density</b>	<b>Open circuit</b>	<b>References</b>
	<b>(mg cm<sup>-2</sup>)</b>	<b>(mW cm<sup>-2</sup>)</b>	<b>potential (V)</b>	
CoTBrPP@bio-C	1.0	100	1.51	This work
CoTPP@bio-C	1.0	86	1.46	This work
Fe <sub>3</sub> N@N-C	1.0	87.5	1.443	21
NP800-VACNT-GF	NA	56	NA	22
Co <sub>3</sub> O <sub>4</sub> nanoplates	2.0	59.7	NA	23
Zn/Co-N@PCNFs-800	1.2	83.5	1.425	24
Cu@Fe-N-C	1.0	92	1.48	25
B <sub>3</sub> N-PG-O-15	1.0	30.43	1.39	26
200-CNTs-Co/NC	1.0	83.1	1.41	27
CF-K-A	1.0	61.5	1.40	28
N-GCNT/FeCo-3	2.0	89.3	1.48	29
25% Cu-N/C	1.0	132	1.40	30
rGO-IL/Mn <sub>3</sub> O <sub>4</sub> (10 : 1)	NA	120	NA	31

<b>Catalyst</b>	<b>Loading</b> <b>(mg cm<sup>-2</sup>)</b>	<b>Peak power density</b> <b>(mW cm<sup>-2</sup>)</b>	<b>Open circuit</b> <b>potential (V)</b>	<b>References</b>
a-MnOx NWs/Ketjblack	NA	190	NA	32
NiCo <sub>2</sub> S <sub>4</sub> /N-CNT	1.0	147	1.49	33
CoO/N-CNT	1.0	265	1.40	34
Co <sub>3</sub> O <sub>4</sub> -SP/NGr-24h	1.0	190	1.52	35
Fe/N/C@BMZIF	1.0	235	1.48	36
S,N-Fe/N/C-CNT	1.25	102.7	1.35	37

Note on table:

(NA)

not

attained.

## References

- 1 V. Mamane, I. Ledoux-Rak, S. Deveau, J. Zyss, O. Riant, *Synthesis*, 2003, **3**, 455-467.
- 2 L. Wang, Y. She, R. Zhong, H. Ji, Y. Zhang, X. Song, *Org. Process Res. Dev.*, 2006, **10**, 757-761.
- 3 L. Chen, Y. Zhang, X. Liu, L. Long, S. Wang, X. Xu, M. Liu, W. Yang, J. Jia, *Carbon*, 2019, **151**, 10-17.
- 4 X. Cui, L. Meng, X. Zhang, X. Wang, J. Shi, *Electrochim. Acta*, 2019, **295**, 384-392.
- 5 J. Zhang, J. Chen, Y. Luo, Y. Chen, X. Wei, G. Wang, R. Wang, *Appl. Surf. Sci.*, 2019, **466**, 911-919.
- 6 J. Chen, X. Wei, J. Zhang, Y. Luo, Y. Chen, G. Wang, R. Wang, *Ind. Eng. Chem. Res.*, 2019, **58**, 2741-2748.
- 7 T. Li, M. Li, M. Zhang, X. Li, K. Liu, M. Zhang, X. Liu, D. Sun, L. Xu, Y. Zhang, Y. Tang, *Carbon*, 2019, **153**, 364-371.
- 8 Q. Wang, L. Shang, R. Shi, X. Zhang, G.I.N. Waterhouse, L.Z. Wu, C.H. Tung, T. Zhang, *Nano Energy*, 2017, **40**, 382-289.
- 9 J. Yin, Y. Li, F. Lv, Q. Fan, Y.Q. Zhao, Q. Zhang, W. Wang, F. Cheng, P. Xi, S. Guo, *ACS Nano*, 2017, **11**, 2275-2283.
- 10 Y. Luo, Z. Wang, Y. Fu, C. Jin, Q. Wei, R. Yang, *J. Mater. Chem. A*, 2016, **4**, 12583-12590.
- 11 L. He, J. Liu, Y. Liu, B. Cui, B. Hu, M. Wang, K. Tian, Y. Song, S. Wu, Z.

- Zhang, Z. Peng, M. Du, *Appl. Catal. B*, 2019, **248**, 366-379.
- 12 H. Guo, Q. Feng, J. Zhu, J. Xu, Q. Li, S. Liu, K. Xu, C. Zhang and T. Liu, *J. Mater. Chem. A*, 2019, **7**, 3664-3672.
- 13 X. Wang, Z. Yang, W. Si, X. Shen, X. Li, R. Li, Q. Lv, N. Wang, C. Huang, *Carbon*, 2019, **147**, 9-18.
- 14 Y. Wang, Y. Pan, L. Zhu, H. Yu, B. Duan, R. Wang, Z. Zhang, S. Qiu, *Carbon*, 2019, **146**, 671-679.
- 15 Y. Hu, D. Huang, J. Zhang, Y. Huang, M.-S. Balogun, Y. Tong, *ChemCatChem*, 2019, DOI: 10.1002/cctc.201901224.
- 16 Z. Xue, J. Kang, D. Guo, C. Zhu, C. Li, X. Zhang, Y. Chen, *Electrochim. Acta*, 2018, **273**, 229-238.
- 17 Z.-H. Xue, H. Su, Q.-Y. Yu, B. Zhang, H.-H. Wang, X.-H. Li, J.-S. Chen, *Adv. Energy Mater.*, 2017, **7**, 1602355.
- 18 Q. Chen, R. Wang, M. Yu, Y. Zeng, F. Lu, X. Kuang, X. Lu, *Electrochim. Acta*, 2017, **247**, 666-673.
- 19 W. Deng, H. Jiang, C. Chen, L. Yang, Y. Zhang, S. Peng, S. Wang, Y. Tan, M. Ma, Q. Xie, *ACS Appl. Mater. Interfaces*, 2016, **8**, 13341-13347.
- 20 Y. Xue, J. Li, Z. Xue, Y. Li, H. Liu, D. Li, W. Yang and Y. Li, *ACS Appl. Mater. Interfaces*, 2016, **8**, 31083-31091.
- 21 T. Li, M. Li, M. Zhang, X. Li, K. Liu, M. Zhang, X. Liu, D. Sun, L. Xu, Y. Zhang, Y. Tang, *Carbon*, 2019, **153**, 364-371.
- 22 X. Cai, L. Lai, L. Zhou, Z. Shen, *ACS Appl. Energy Mater.*, 2019, **2**, 1505-1516.

- 23 P. Tan, B. Chen, H. Xu, W. Cai, W. He, M. Ni, *Energy*, 2019, **166**, 1241-1248.
- 24 Q. Niu, B. Chen, J. Guo, J. Nie, X. Guo, G. Ma, *Nano-Micro Lett.*, 2019, **11**, 8.
- 25 Z. Wang, H. Jin, T. Meng, K. Liao, W. Meng, J. Yang, D. He, Y. Xiong, S. Mu, *Adv. Funct. Mater.*, 2018, **28**, 1802596.
- 26 L. Qin, L. Wang, X. Yang, R. Ding, Z. Zheng, X. Chen, B. LV, *J. catal.*, 2018, **359**, 242-250.
- 27 S. Liu, I.S. Amiin, X. Liu, J. Zhang, M. Bao, T. Meng, S. Mu, *Chem. Eng. J.*, 2018, **342**, 163-170.
- 28 J. Zhu, W. Li, S. Li, J. Zhang, H. Zhou, C. Zhang, J. Zhang, S. Mu, *Small*, 2018, **14**, 1800563.
- 29 C.-Y. Su, H. Cheng, W. Li, Z.-Q. Liu, N. Li, Z. Hou, F.-Q. Bai, H.-X. Zhang, T.-Y. Ma, *Adv. Energy Mater.*, 2017, **7**, 1602420.
- 30 Q. Lai, J. Zhu, Y. Zhao, Y. Liang, J. He and J. Chen, *Small*, 2017, **13**, 1700740.
- 31 J.-S. Lee, T. Lee, H.-K. Song, J. Cho and B.-S. Kim, *Energy Environ. Sci.*, 2011, **4**, 4148-4154.
- 32 J.-S. Lee, G.S. Park, H.I. Lee, S.T. Kim, R. Cao, M. Liu and J. Cho, *Nano Lett.*, 2011, **11**, 5362-5366.
- 33 X. Han, X. Wu, C. Zhong, Y. Deng, N. Zhao, W. Hu, *Nano Energy*, 2017, **31**, 541-550.
- 34 Y. Li, M. Gong, Y. Liang, J. Feng, J.-E. Kim, H. Wang, G. Hong, B. Zhang and H. Dai, *Nat. Commun.*, 2013, **4**, 1805.
- 35 S.K. Singh, V.M. Dhavale and S. Kurungot, *ACS Appl. Mater. Interfaces*, 2015, **7**,

21138-21149.

36 M. Wang, T. Qian, J. Zhou and C. Yan, *ACS Appl. Mater. Interfaces*, 2017, **9**, 5213-5221.

37 P. Chen, T. Zhou, L. Xing, K. Xu, Y. Tong, H. Xie, L. Zhang, W. Yan, W. Chu, C. Wu and Y. Xie, *Angew. Chem. Int. Ed.*, 2017, **56**, 610-614.